Paving the way for cristobalite TiO_2 and GeO_2 attainable under moderate tensile stress: A DFT study of transformation paths and activation barriers in cristobalite-rutile transformations of MO_2 (M = Si, Ge, Ti)

Shariq Haseen, Peter Kroll*

Department of Chemistry and Biochemistry, The University of Texas at Arlington, 700 Planetarium Place, Arlington, TX 76019, United States

ABSTRACT

We investigate energetics of interconversions between cristobalite-type and rutile-type structures of SiO_2, GeO_2, and TiO_2 at different pressures within Density Functional Theory. Cristobalite-SiO_2 is succeeded by the rutile-type, stishovite-SiO_2, at high pressures. The rutile-types of GeO_2 and TiO_2 are favored at ambient pressure, but small tensile stresses are sufficient to yield cristobalite-GeO_2 and TiO_2. The transition from one structure-type into the other is modeled using collective movements of cations or anions with different degrees of freedom for the remaining structure parameters. We find that increasing the external pressure decreases activation barriers of the cristobalite-rutile transformation. Activation barriers of the reverse transformation from rutile to critobalite decrease with decreasing pressure. If only a fraction of cations follows the collective movement we find even lower activation barriers. The final states are still tetrahedrally or octahedrally coordinated structures, albeit not the high-symmetry variants of cristobalite or rutile, respectively. The small tensile stresses needed to favor cristobalite-GeO_2 and TiO_2 over their respective rutile counterparts, and the low activation barriers involved in their interconversion let us propose a simple route to synthesize cristobalite-GeO_2 and a new cristobalite-TiO_2.

1. Introduction

Transformations between structures described using the concepts cubic-closest packing (ccp) and hexagonal closest packing (hcp) are standard topics in metallurgy and crystal chemistry [1]. Many of them proceed or are activated at high temperature and/or high pressure. A particular example is the transformation between cristobalite-type and rutile-type structures. Anions in cristobalite are approximately ccp with cations filling tetrahedral interstitials while those in rutile are approximately hcp with cations in octahedral interstitials. The binary oxides silica (SiO_2) and germania (GeO_2) both exhibit cristobalite-type and rutile-type polymorphs [2–7]. SiO_2 α-cristobalite has many industrial uses [8] and stishovite is one of the hardest known oxides [9]. A natural source for GeO_2 cristobalite has not been discovered so far, but synthesis of GeO_2 cristobalite has been reported [5–7]. However, extensive characterization of GeO_2 cristobalite has not been reported, and its existence as a pure phase has even been disputed [10]. Rutile GeO_2 is the most stable GeO_2 polymorph at ambient conditions and has potentially useful optical properties [11]. The eponymous rutile is a polymorph of titania (TiO_2) [12] and well-known for its use as white pigment [13,14] Additional applications range from (photo)catalysis to

energy storage [15,16]. A cristobalite-TiO_2 has not yet been synthesized or found in nature.

Previous studies investigated the transformation between SiO_2 cristobalite and stishovite. O'Keefe and Hyde proposed a reaction mechanism by which α-cristobalite transforms to rutile-type via rotation of SiO_4 tetrahedra and simultaneous displacement of cations and anions [17]. This path was studied later by Silvi et al. using Hartree-Fock calculations [18]. Klug et al. were the first to simulate the pressure-induced transformation from cristobalite to stishovite using ab initio constant pressure molecular dynamics (MD) [19]. Analysis of atomic trajectories during the transformation revealed a smooth structural evolution from cristobalite to stishovite similar to the transition path proposed by O'Keefe and Hyde. No intermediate structure of lower symmetry was reported. Huang et al. used a very similar method to study the transition in dynamic simulations [20]. Their study corroborated the transition path of O'Keefe and Hyde but indicated unquenchable intermediate structures along the pathway. Salvadó et al. followed the cristobalite-rutile transformation for SiO_2 within Density Functional Theory (DFT) using a common sub-group and applied a concerted movement of cations along the proposed transition path [21]. Their study yielded a smooth energy profile without intermediate local

minima. We had previously performed a similar study of the cristobalite-rutile transition in SiO_2 and TiO_2, but followed a concerted movement of anions along the proposed transition path instead [22].

The goal of this paper is to provide a comparative study of the transformation from cristobalite to rutile for SiO_2, GeO_2, and TiO_2. We provide transition pressures and compare enthalpy profiles and activation energies for the concerted movements by cations and by anions. We indicate that intermediate structures may occur if only a fraction of cations move in a concerted way. Anticipating our results, we will show for both GeO_2 and TiO_2 that transformation from a rutile structure to cristobalite requires only moderate tensile stresses, and experimental realization should be feasible.

2. Method

All calculations are done within Density Functional Theory as implemented in the Vienna *ab initio* Simulation Package (VASP) [23–26]. For electron exchange and correlation we use the Generalized Gradient Approximation as parametrized by Perdew, Becke, and Ernzerhof (PBE) [27,28]. For comparison, we apply the Strongly Constrained and Appropriately Normed (SCAN) functional [29]. Atom cores are described through the projector augmented wave (PAW) method [30,31]. A 4x4x4 mesh is used for all structures to sample the Brillouin zone [32]. Energies are converged to 0.01 meV/atom and forces to 5 meV/Å.

After optimization of structures we compute the energy of each model for a series of volumes around the minimum configuration. At each step the structure is optimized under the constraint of constant volume. The resulting energy-volume data for each structure is transformed into enthalpy-pressure data by numerically differentiating a spline fit to the data. Points of equal enthalpy then define the transition pressure p_t of the transition from the α-cristobalite-type to the rutile-type. In the case of SiO_2, p_t is positive, while for GeO_2 and TiO_2 p_t is negative.

2.1. Structures and transition paths

The structure of α-cristobalite MO_2 (M = Si, Ge, Ti) is built up by corner-connected MO_4 tetrahedra. Its topology resembles that of the diamond network, with two-connected O atoms bridging between vertices of the diamond structure. The O atoms in α-cristobalite fall, approximately, on sites of a cubic-closest-packed structure. For SiO_2 and GeO_2 the optimized α-cristobalite structure exhibits bending of the angle at O, while for TiO_2 the bond angle is almost 180°. Hence, TiO_2 optimizes towards the (ideal) β-cristobalite structure [33]. The rutile structure, as realized in stishovite-SiO_2 as well as rutile-GeO_2 and TiO_2, comprises MO_6-octahedra sharing edges. O atoms are three-fold coordinated and fall, approximately, on sites of a hexagonal-closest packed structure.

With their resemblance to ccp (cristobalite) and hcp (rutile), a simple transformation path between cristobalite and rutile can be constructed following standard concepts of metallurgy and crystal chemistry [17]. Using a common space group $C222_1$ (20), the two structures can be described using the parameters shown in Table 1. Note that $C222_1$ is an orthorhombic space group, but representation of both tetragonal structures in $C222_1$ will relate lattice parameter a and b. The different Wyckhoff positions (4b for Si1, 4a for Si2, 8c for O1 and O2) account for 8 independent position parameters, but representation of α-cristobalite in $C222_1$ requires only 4 independent position parameters, that of rutile just one position parameter. Data of all parameters is provided in Table 2 in the results section.

Using the common space group representation and correspondence between lattice parameters and coordinates, a transformation between cristobalite and rutile is facilitated by interpolating between structure parameters of both structures. In general, intermediate configurations have the full freedom of parameters as allowed in space group $C222_1$. The interpolation can happen in different ways, for example by linear

Table 1
Generic description of lattice parameters and coordinates of cristobalite-type and rutile-type structures using the common space group $C222_1$ (20). The Wyckhoff positions of $C222_1$ are *4a* (x,0,0), *4b* (0,y,1/4), and *8c* (x,y,z). Our choice of parameters (e.g. 1 rather than 0) allows to describe the transition between of cristobalite and rutile by interpolation between the respective parameters while maintaining $C222_1$ symmetry.

a,b,c		cristobalite-type			rutile-type		
		a_c	a_c	c_c	a_s	a_s	c_s
	Wyckhoff	x	y	z	x	y	z
Si1	*4b*	0	y_cSi	1/4	0	1/2	1/4
Si2	*4a*	y_cSi+1/2	0	0	1	0	0
O1	*8c*	x_cO	y_cO	z_cO	0	y_sO	1/2
O2	*8c*	y_cO	1/2-x_cO	z_cO-1/4	y_sO	1/2	1/4

Table 2
Lattice parameters and internal parameters of $C222_1$ cristobalite-type and rutile-type SiO_2, GeO_2, TiO_2 from structures optimized with PBE and SCAN functionals. [a][35], [b][36], [c][37], [d][38], [e][39]

		Cristobalite-type				Rutile-type		
		Exp.	PBE	SCAN		Exp.	PBE	SCAN
SiO_2	a_c (Å)	7.0400[a]	7.2270	7.0680	a_s (Å)	5.9110[c]	5.9900	5.9140
	c_c (Å)	6.9321[a]	7.1520	6.9580	c_s (Å)	5.3338[c]	5.3880	5.3400
	y_cSi	0.3008[a]	0.2909	0.3000				
	x_cO	0.0680[a]	0.0777	0.0679				
	y_cO	0.1719[a]	0.1646	0.1714	y_sO	0.30613[c]	0.3069	0.3064
	z_cO	0.4287[a]	0.4207	0.4282				
GeO_2	a_c (Å)	7.06[b]	7.2240	7.0160	a_s (Å)	6.2177[d]	6.3690	6.2530
	c_c (Å)	7.06[b]	7.3870	7.1800	c_s (Å)	5.7252[d]	5.8580	5.7800
	y_cGe	0.328[b]	0.3201	0.3291				
	x_cO	0.0445[b]	0.0324	0.0244				
	y_cO	0.211[b]	0.1945	0.2002	y_sO	0.3063[d]	0.3067	0.3058
	z_cO	0.465[b]	0.4562	0.4594				
TiO_2	a_c (Å)		8.4740	8.4210	a_s (Å)	6.49641[e]	6.5980	6.5200
	c_c (Å)		8.4680	8.4230	c_s (Å)	5.91736[e]	5.9390	5.9130
	y_cTi		1/2	1/2				
	x_cO		0.1203	0.1225				
	y_cO		0.1295	0.1274	y_sO	0.3048[e]	0.3048	0.3042
	z_cO		0.3796	0.3775				

interpolation of all parameters simultaneously [17]. Two other modes of concerted movement of all atoms are studied here. In the "anion method," positions of the anions as well as cell parameters are linearly interpolated between cristobalite and rutile. Hence, starting from one structure, the anion positions and lattice parameters are progressively moved forward and kept fixed. The cations are allowed to optimize, conforming to each new configuration. In the next step, anions are moved forward again, and cations positions of the previous intermediate are used as starting point for the optimization. Previously, we had investigated this path for the transformation in SiO_2 [22]. In the "cation method", positions of cations are linearly interpolated between initial and final configurations, while the anions are allowed to optimize, conforming to each new configuration. In addition, at each intermediate step the cell parameters are allowed to optimize according to the given constraints. This latter approach has recently been investigated for transitions in SiO_2 by Salvadó et al. [21]. Note that the paths described above retain space group $C222_1$ during the transformation. "Cation method" and "anion method" are barely distinguishable by viewing intermediate structure. However, computed energy profiles are noticeably different as are distances between atoms. This will be discussed further below. For both approaches we use 19 intermediate configurations. The small step size between intermediates guarantees a smooth connection and no significant jumps of atoms from one optimized step to the next one.
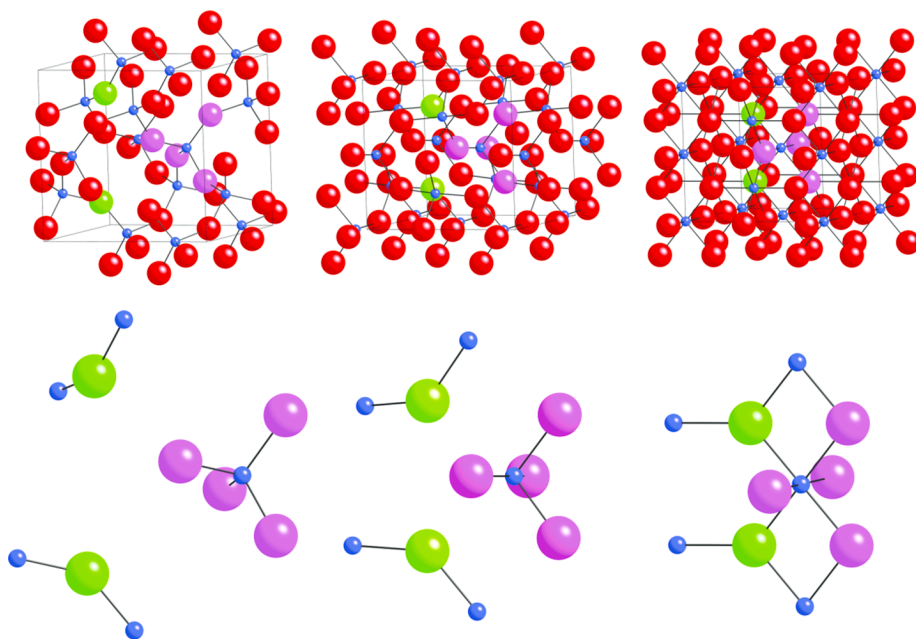
Fig. 1. Initial (top left), intermediate (top middle) and final (top right) step of the transformation path from cristobalite to rutile. The orthorhombic common unit cell (SpGr. $C222_1$) is outlined. Si atoms are blue and O atoms are red. For one Si we highlight its initially four (4) coordinating oxygen neighbors (purple) and the two additional oxygen (green) approaching it to form the final SiO_6-octahedron. Enlarged views of the forming octahedral SiO_6 during the transformation are shown directly beneath the corrseponding step in the transformation path [34]. (For interpretation of the references to colour in this figure legend, the reader is referred to the web version of this article.)

The concerted movement of atoms as described above causes a rotation of MO_4 tetrahedra in cristobalite. This goes along with their slight deformation and, due to the volume contraction and increasing density, with the approach of two additional anions towards the cation center, see Fig. 1. This forms MO_6 octahedra characteristic for the rutile structure. Note that on the path from cristobalite to rutile no bond is broken, but two additional bonds per cation are formed. Conversely, the reverse path from rutile to cristobalite breaks two Si-O bonds.

3. Results and discussions

Optimizing the structures using PBE and SCAN functionals yields parameters listed in Table 2. Energy and energy differences between the optimized (local) ground state structures as well as computed transition pressures are given in Table 3. Comparing results achieved with both functionals, we note that the SCAN functional appears to "favor" higher coordination of cations in the octahedrally coordinated structure. For instance, α-cristobalite-SiO_2 is more favorable than stishovite (which is rutile-SiO_2). Within PBE the energy difference is 0.58 eV/SiO_2, while using SCAN this comes up to only 0.39 eV/SiO_2. For both GeO_2 and TiO_2 the rutile structure is more favorable than the cristobalite-type. Computed energy differences for GeO_2 are -0.16 eV/GeO_2 (PBE) and -0.41 eV/GeO_2 (SCAN), and for TiO_2 they are -0.09 eV/TiO_2 (PBE) and -0.52 eV/TiO_2 (SCAN). Consequently, transition pressures p_t computed by computed using PBE are systematically 1.5–2 GPa higher than transition pressures SCAN (see Table 3).

Table 3
Optimized energies of cristobalite-type and rutile-type SiO_2, GeO_2, and TiO_2 at ambient pressure, energy differences ΔE from cristobalite-type to rutile-type, and computed transition pressures p_t found using PBE and SCAN functionals.

	Cristobalite-type (eV/f.u.)	Rutile-type (eV/f.u.)	ΔE (eV/f.u.)	p_t (GPa)
PBE				
SiO_2	-23.74	-23.16	0.58	5.4
GeO_2	-19.01	-19.17	-0.16	-1.4
TiO_2	-26.32	-26.41	-0.09	-0.4
SCAN				
SiO_2	-31.57	-31.21	0.36	3.2
GeO_2	-36.52	-36.93	-0.41	-3.3
TiO_2	-37.53	-38.05	-0.52	-1.9

The reason for reduced transition pressures is related to the (partial) inclusion of short range van-der-Waals interactions in SCAN [40]. This is corroborated by adding van-der-Waals interactions to the PBE functional. We choose the universal low gradient correction (ulg) together with the PBE functional, thus performing PBE + ulg calculations [41]. For the α-cristobalite to stishovite of SiO_2 we then receive a transition pressure of 2.0 GPa, even lower than for SCAN (3.2 GPa) and significantly reduced in comparison to "standard" PBE calculations (5.4 GPa). Very similar trends are found for GeO_2 and TiO_2 as well.

We present the energy-volume graphs for SiO_2, GeO_2, and TiO_2 computed using PBE and SCAN in Fig. 2. It is apparent for each compound that the rutile-type structure has a higher curvature around the energy minimum than the cristobalite-type. Therefore, the rutile-type structure is less compressible. The very shallow E-V curve of the cristobalite-type is indicative of the shallow potential energy surface for bending the M–O–M bond angle at O [42]. Converting the energy-volume (E-V) data into relative enthalpy-pressure (ΔH-p) diagrams computed yields the diagrams shown in Fig. 3, from which we determine transitions pressures as collected in Table 3.

Our results for the cristobalite-stishovite transition are aligned with previous studies, which found a transition pressure of 5–6 GPa [18,21,22]. Experimentally, a conversion from cristobalite to stishovite is feasible between 10 and 15 GPa, but intermediate phases may appear depending on exact temperature-pressure conditions [43–45].

Since for both GeO_2 and TiO_2 the rutile structure is more favorable at ambient pressure, we compute negative pressures for a transition from rutile to cristobalite. In the case of GeO_2 values of p_t are -1.4 GPa (PBE) and -3.3 GPa (SCAN). Saito and Ono previously computed polymorphs of GeO_2 and their data yields $p_t \approx -6$ GPa [46]. Yamaguchi et al. reported that cristobalite-GeO_2 transforms into rutile-GeO_2 through just grinding of the material [7]. On the other side, rutile-GeO_2 transforms into α-quartz-GeO_2 at 1340 K at ambient pressure, supporting a small enthalpy difference between octahedral and tetrahedral polymorphs of GeO_2 [47,48]. Given that for TiO_2 we compute even smaller transition pressures (PBE: -0.4 GPa; SCAN: -1.9 GPa) than for GeO_2, a transition of rutile into a structure with tetrahedral TiO_4–units should be feasible.

Negative pressures correspond to isotropic tensile stresses and have been realized by mixing materials with differing crystal structures [49]. Yet another approach is the synthesis of a material or composite under compressive stress and subsequent relaxation. This can be achieved, for
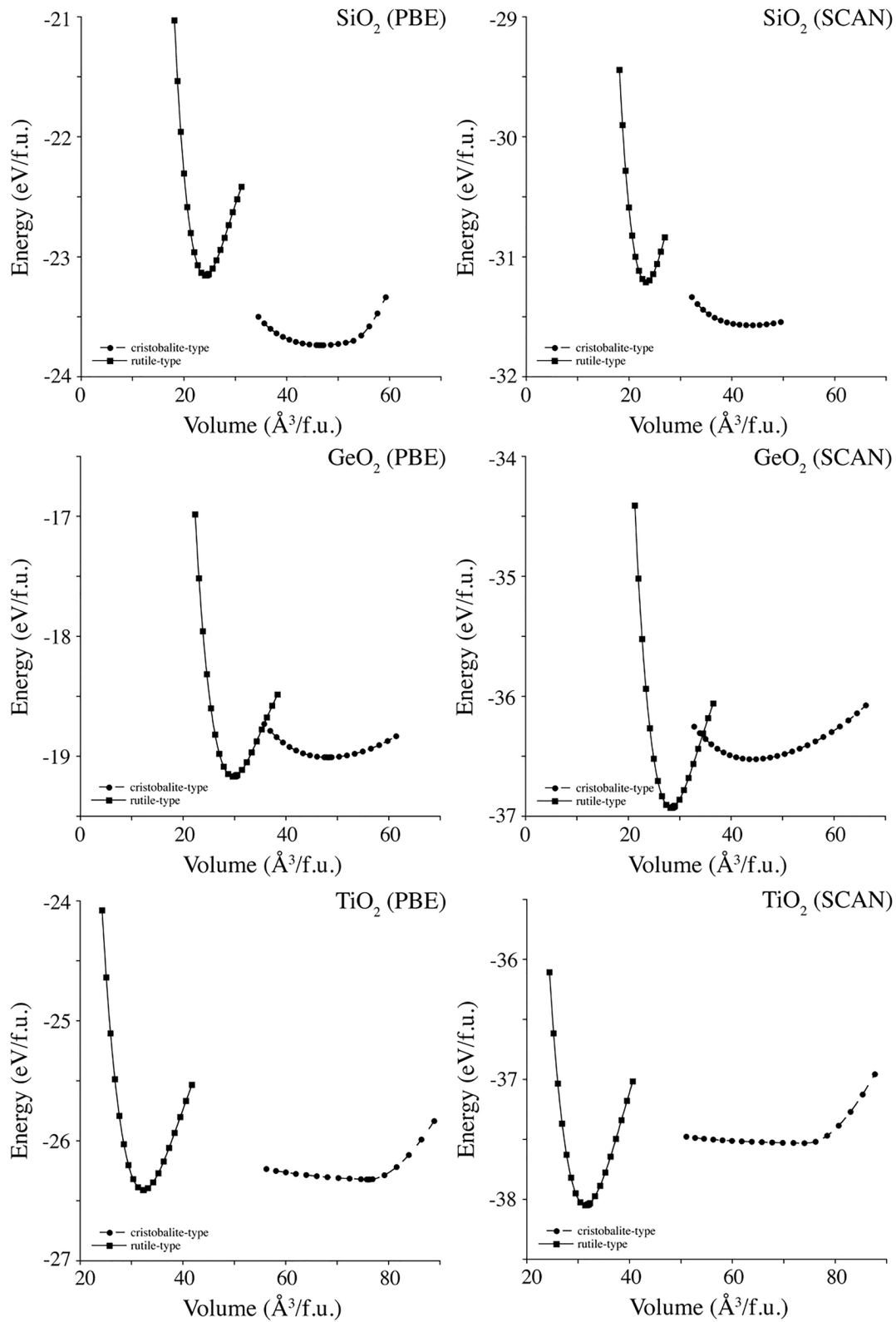
Fig. 2. E-V diagrams with quantities given per formula unit (f.u.) for cristobalite-type and rutile-type SiO_2, GeO_2, and TiO_2 using PBE (left) and SCAN (right) functionals.

instance, by thin film deposition on a bent substrate. Stress-relief of the substrate will in turn induce (negative) tensile stresses on the film. Stresses in the range of 5 GPa are quite commonly occurring in thin film depositions [50,51]. The rate of a transition and, thus, whether the two

polymorphs, cristobalite and rutile, can practically be converted into one another, depends on the activation energy required for the process. Hence our further investigations address the energy profile of a transition between cristobalite- and rutile-type structures.
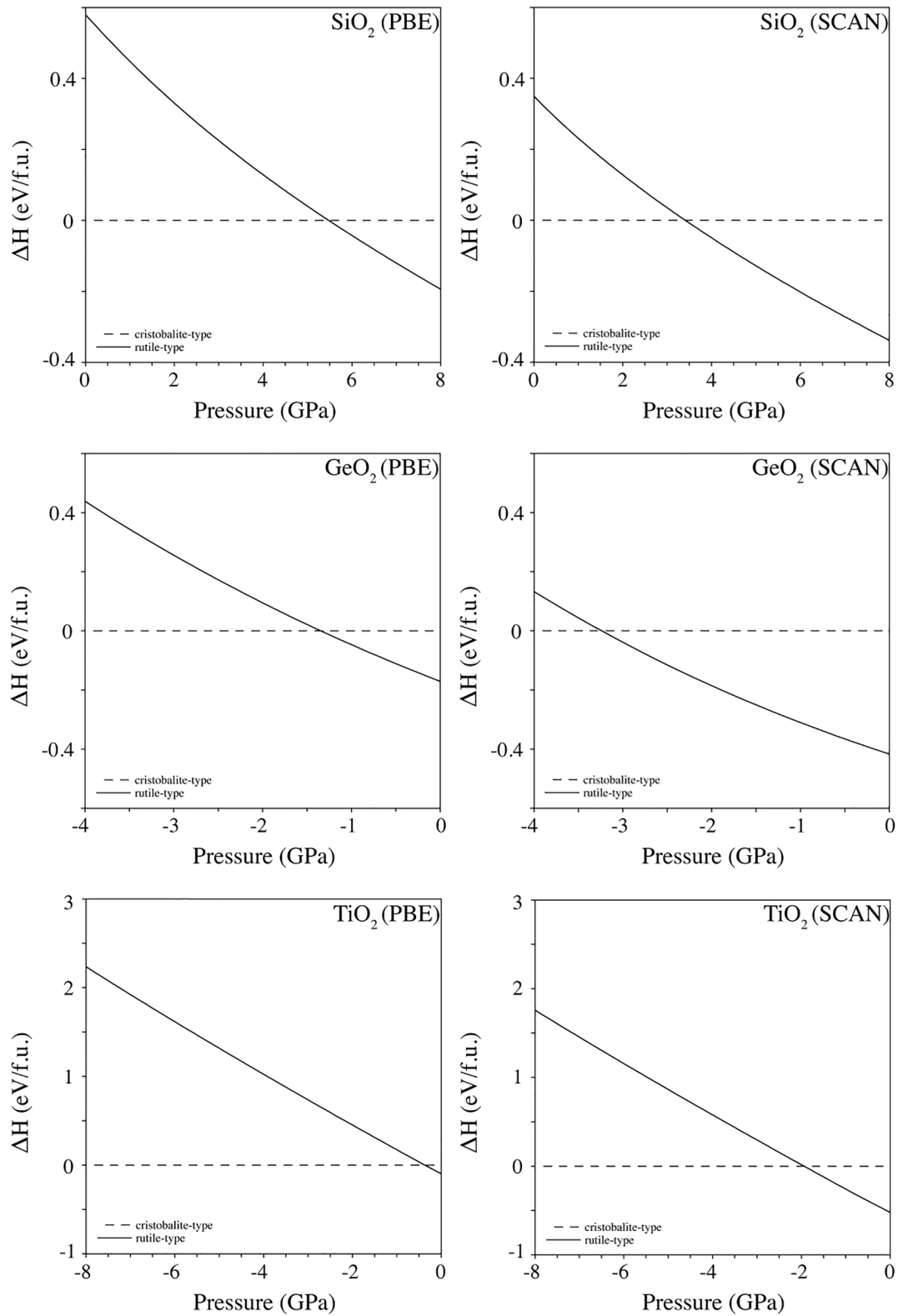
Fig. 3. Enthalpy-pressure diagrams for MO_2 (M = Si, Ge, Ti) relative to enthalpy of corresponding cristobalite-type using PBE and SCAN functionals. Cristobalite-rutile transition pressures are found at intersections of enthalpy curves.

3.1. Transformation profiles between cristobalite and rutile at different pressures

We then set out and computed the enthalpy profile for the transformation from cristobalite-type to rutile-types structure for each compound. The forward transition starts with the optimized structures of cristobalite-types of SiO_2, GeO_2, and TiO_2, while the reverse transition starts with the rutile-type of each compound. We explicitly computed both directions of the transition path, forward and reverse, for each method and received matching energy profiles. We computed

transition paths at ambient pressure (0 GPa), at the computed transition pressures (see Table 3), and at a few additional pressures to highlight trends. If a transition was performed at a given pressure, we selected optimized geometries of initial and final structures accordingly.

The enthalpy profile of a transition path reflects the enthalpy differences cristobalite- and rutile-type structures for a given MO_2 compound at a given pressure. Thus, at ambient pressure (0 GPa) initial and final state are energetically different according to the data of Table 3. At transition pressure p_t, however, cristobalite- and rutile-type have equal enthalpy and appear at level with each other. All transition paths provide a configuration with maximum enthalpy, the transition state. The activation barrier for the forward reaction, $\Delta H_{a,fwd}$, is defined as the enthalpy difference between cristobalite and the transition state. Conversely, the difference between rutile and the transition state constitutes the activation barrier for the reverse reaction, $\Delta H_{a,rev}$. We have chosen to plot the energy profiles relative to the structure with lowest energy at ambient pressure. Thus, for SiO_2 we plot the profile relative to cristobalite-type, while for GeO_2 and TiO_2 we plot all profiles relative to the rutile type.

3.2. SiO_2

The energy profiles for the two different paths to convert α-cristobalite to stishovite are shown in Fig. 4. Enthalpy barriers for the

Table 4
Forward activation enthalpies $\Delta H_{a,fwd}$ for SiO_2 cristobalite-rutile transformations. The asterisk (*) indicates the transition pressure computed in the respective method.

Pressure (GPa)	Anion method $\Delta H_{a,fwd}$ (eV/f.u.)	Cation method $\Delta H_{a,fwd}$ (eV/f.u.)
PBE		
−5.0	2.42	2.07
−2.0	1.90	1.57
0	1.57	1.28
5.4*	1.01	0.81
20.	0.39	0.22
30.	0.17	0.04
SCAN		
0	1.44	1.16
3.2*	1.09	0.88

forward path, $\Delta H_{a,fwd}$, at different pressures are listed in Table 4. For paths computed at 0 GPa in both anion and cation method, we investigated the transition state in more detail and computed the Hessian matrix. It exhibits only a single imaginary eigenvalue, and the corresponding eigenvector aligns with conservation of space group symmetry $C222_1$. Overall we find that the cation method produces slightly lower enthalpies, and consequently lower $\Delta H_{a,fwd}$, in comparison to the

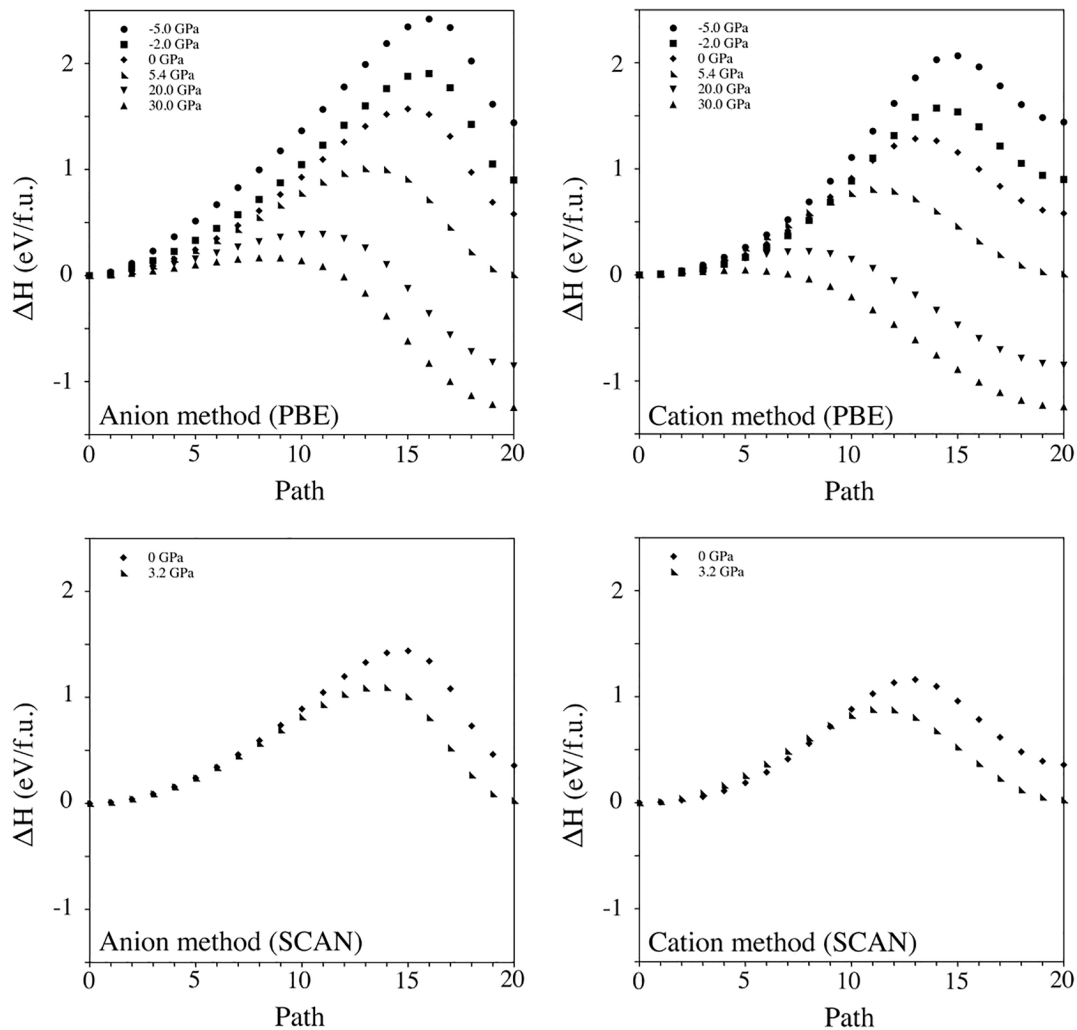**Fig. 4.** Enthalpy profiles of SiO_2 α-cristobalite (step = 0) to stishovite (step = 20) transition at various pressures. PBE calculations for (top left) anion and (top right) cation method; SCAN calculations for (bottom left) anion and (bottom right) cation method. All enthalpies are given relative to α-cristobalite SiO_2 at the corresponding pressure.

anion method. This occurs because more degrees of freedom, three position parameters and two cell parameters, are allowed to relax in this approach. In the anion method, we allow only one position parameter to optimize, while all other parameters are interpolated. We also observe that increasing pressure reduces the enthalpy barrier of the forward path, $\Delta H_{a,fwd}$, in either method and in both PBE and SCAN calculations.

Eventually the activation energy $\Delta H_{a,fwd}$ approaches zero (0) at 30 GPa. In experiments, α-cristobalite-SiO$_2$ completely amorphizes at about 28 GPa [52]. Comparing the two functionals we find that SCAN calculations yield slightly lower activation energies than their PBE counterparts; at ambient pressure $\Delta H_{a,fwd}$ is about 10% lower. For the transition pressure p_t itself, however, $\Delta H_{a,fwd}$ computed in SCAN is slightly higher, because SCAN computes lower transition pressures in general. Conversely, the higher transition pressure p_t obtained with the PBE functional impacts the energy profile and yields a lower $\Delta H_{a,fwd}$ at p_t.

3.3. GeO$_2$

The energy profiles for the transition paths from an α-cristobalite-type to rutile-type GeO$_2$ are shown in Fig. 5. Note that we depict enthalpy relative to rutile GeO$_2$ (see Table 5), since this is lower in energy at ambient pressure than cristobalite GeO$_2$. Consequently, we address

Table 5
Reverse activation enthalpies $\Delta H_{a,rev}$ for GeO$_2$ cristobalite-rutile transformations. The asterisk (*) indicates the transition pressure computed in the respective method.

Pressure (GPa)	Anion method $\Delta H_{a,rev}$ (eV/f.u.)	Cation method $\Delta H_{a,rev}$ (eV/f.u.)
PBE		
0	0.84	0.62
−1.4*	0.83	0.60
SCAN		
0	0.94	0.74
−3.3*	0.95	0.66

$\Delta H_{a,rev}$, the enthalpy barrier for the reverse path. Again, the cation method yields lower enthalpy profiles and lower $\Delta H_{a,rev}$ in comparison to the anion method. An impact of pressure on the energy profile is best seen within the cation method. Decreasing the pressure lowers the energy profile and, as a consequence, yields a lower $\Delta H_{a,rev}$ at negative pressure. Comparing PBE and SCAN calculations we find that SCAN calculations in case of GeO$_2$ yield higher activation energies than their PBE counterparts, about 20% at ambient pressure. Even at the transition pressure, which SCAN locates at larger negative pressure than PBE, there is still a 10% difference.
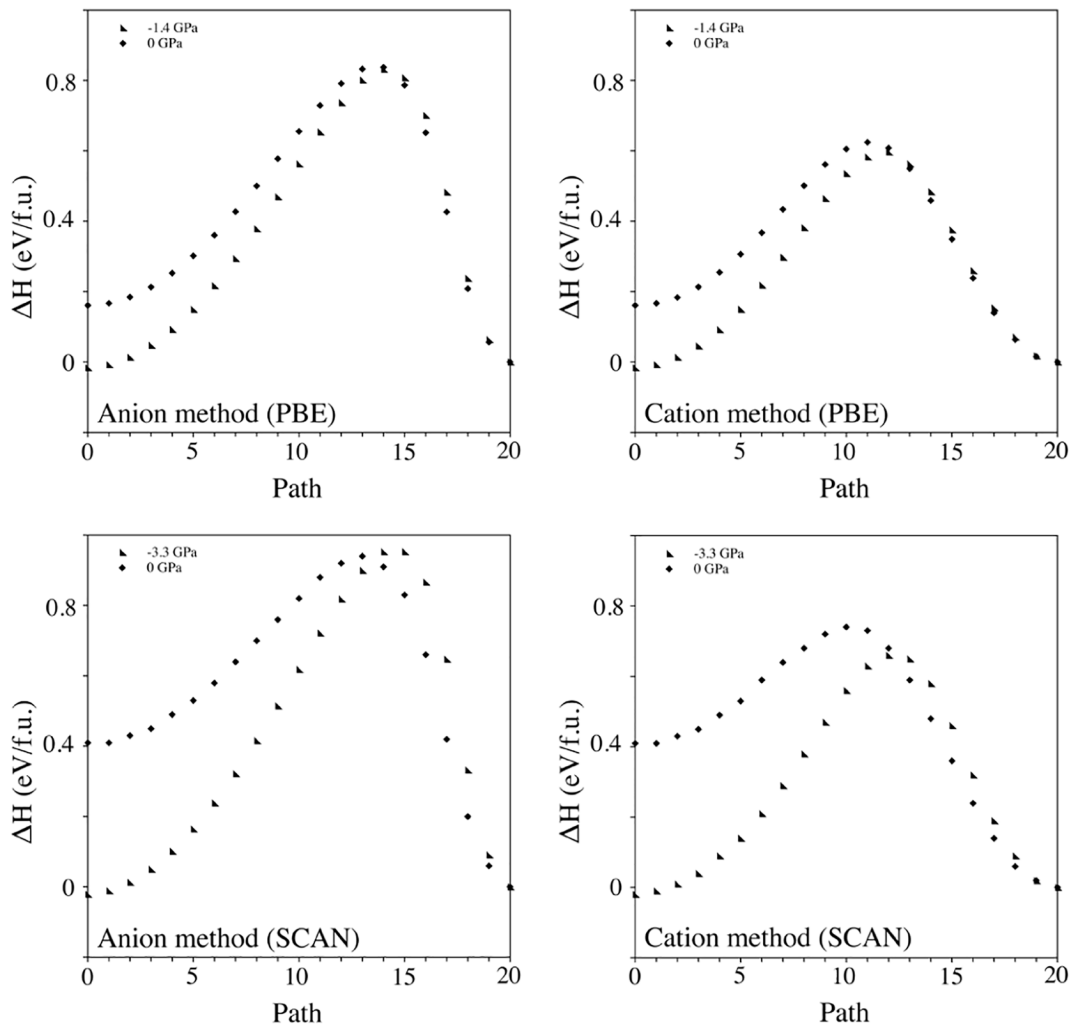

Fig. 5. Enthalpy profiles of GeO$_2$ α-cristobalite (step = 0) to rutile (step = 20) transition at ambient and transition pressure p_t. PBE calculations for (top left) anion and (top right) cation method; SCAN calculations for (bottom left) anion and (bottom right) cation method. All enthalpies are given relative to rutile GeO$_2$ at corresponding pressure.
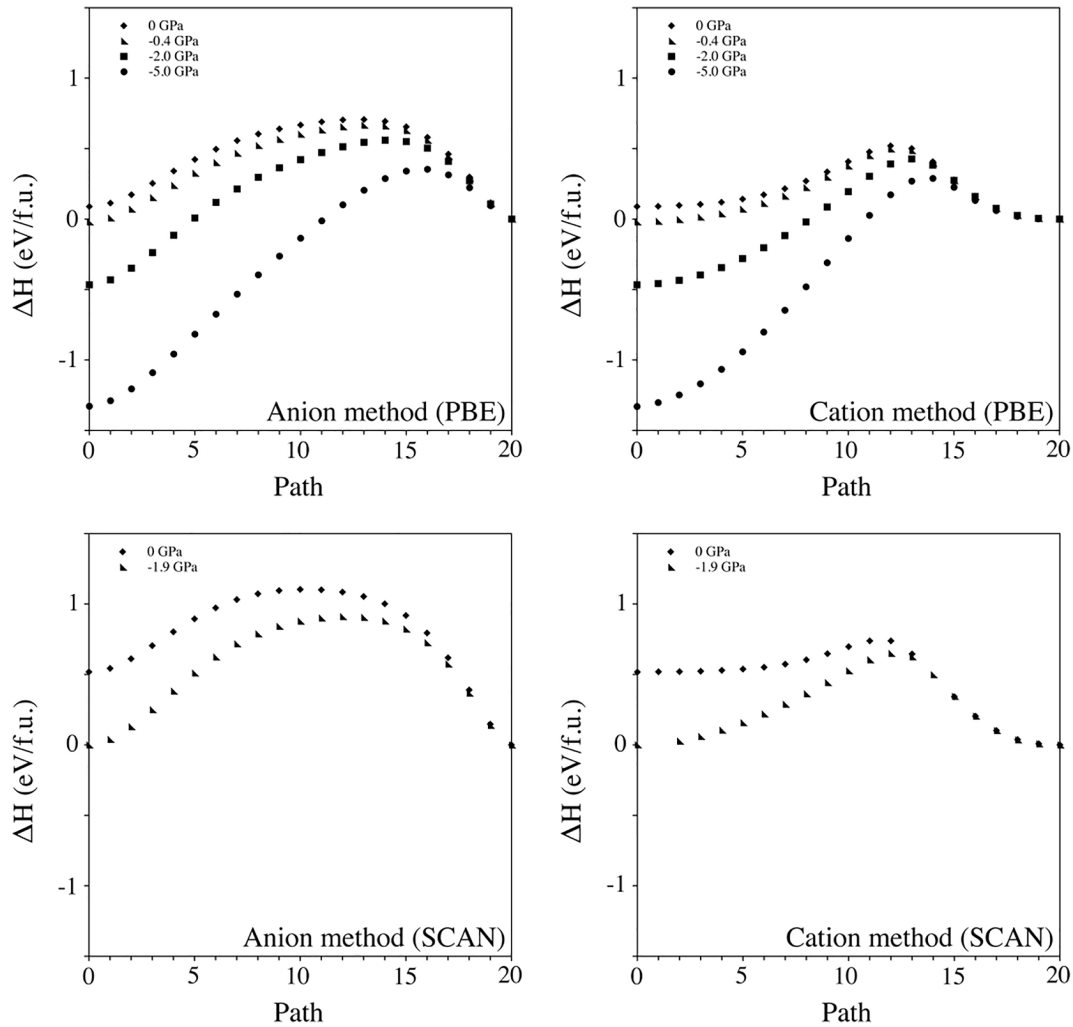
Fig. 6. Enthalpy profiles of TiO_2 α-cristobalite (step = 0) to rutile (step = 20) transition at ambient and transition pressure p_t. PBE calculations for (top left) anion and (top right) cation method; SCAN calculations for (bottom left) anion and (bottom right) cation method. All enthalpies are given relative to rutile TiO_2 at corresponding pressure. Two points in the diagram for cation method with SCAN (step 1 at −1.9 GPa and step 14 at 0 GPa) could not be optimized.

3.4. TiO_2

The energy profiles for the transition paths from an α-cristobalite-type to rutile-type TiO_2 are shown in Fig. 6. We depict enthalpy relative to rutile TiO_2 and address the enthalpy barrier $\Delta H_{a,rev}$ of the reverse path (see Table 6). Once more, the cation method yields lower enthalpy profiles and lower $\Delta H_{a,rev}$ in comparison to the anion method. Reducing pressure significantly lowers the energy profile and, as a consequence, yields a a lower $\Delta H_{a,rev}$. Like with GeO_2, SCAN calculations yield higher

Table 6
Reverse activation enthalpies $\Delta H_{a,rev}$ for TiO_2 cristobalite-rutile transformations. The asterisk (*) indicates the transition pressure computed in the respective method.

Pressure (GPa)	Anion method $\Delta H_{a,rev}$ (eV/f.u.)	Cation method $\Delta H_{a,rev}$ (eV/f.u.)
PBE		
−5.0	0.35	0.29
−2.0	0.56	0.43
−0.4*	0.69	0.50
0	0.71	0.52
SCAN		
−1.9*	0.91	0.65
0	1.10	0.74

activation energies (about 40%) than their PBE counterparts. Independent of the path selected, however, going from ambient (0 GPa) to −5 GPa essentially cuts the activation barrier in half. Thus, negative pressure not only favors the cristobalite-type of TiO_2, but also makes it more easily accessible within this transformation.

3.5. Further reducing degrees of freedom during transformations

The cation method and anion method are distinguished by the number of constraints implied and by the degrees of freedoms optimized at every step. Overall, the cation method yields lower activation barriers, because at every step more atom coordinates as well as the lattice parameters can relax. It is, therefore, of interest to see, if we can put even less constraints onto the transition and what enthalpy profile this would yield. Starting with the same size of the simulation cell, 8 cations and 16 anions in space group $C222_1$, we extended the cation method in such a way as we did not impose any symmetry constraint ($P1$) and, furthermore, allowed half of the cations to optimize during the transformation as well. Thus, a concerted motion is only provided by 4 cations, while all other atoms and cell parameters optimize in each intermediate step. Among the possible scenarios resulting from this approach are yet again transition paths from cristobalite to rutile and vice-versa, but with even lower energy at respective transition states due to increased degrees of freedom. Other potential outcomes may
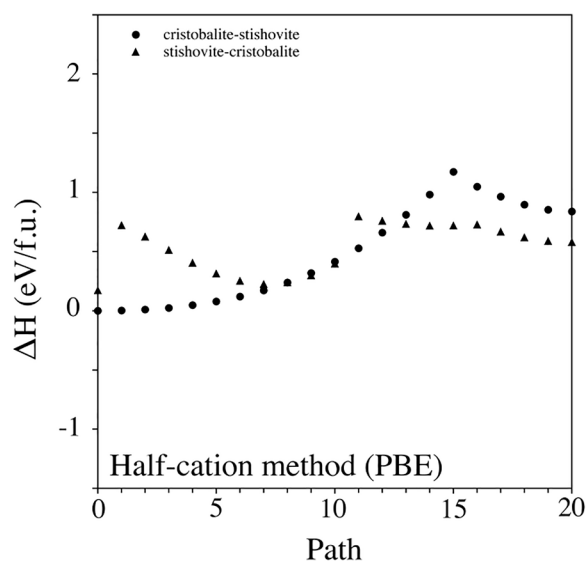
Fig. 7. Enthalpy profiles of transformations from cristobalite-SiO$_2$ to stishovite-SiO$_2$ and stishovite-SiO$_2$ to cristobalite-SiO$_2$; transformations were done at zero pressure with PBE using the half-cation method. Enthalpies are relative to the enthalpy of α-cristobalite-SiO$_2$.

yield small ordered clusters or nuclei of either structure embedded in a disordered matrix or even completely disordered structures with broken and dangling bonds. We investigated the path for SiO$_2$ at ambient pressure (0 GPa) with two different selections of a group of 4 cations, of which we will display the results of one only. The second choice had, essentially, very similar consequences.

Two energy profiles of this "half-cation method" are shown in Fig. 7. Both energy profiles show cusps, indicating a discontinuity of the derivative of energy along the transition path. This is in contrast to all profiles shown previously, which were smooth and continuous. Even when using a five-times finer interpolation around the critical points the discontinuities remain. Indeed, at these points bonds break (stishovite-cristobalite) or form (cristobalite-stishovite) and displacements of some atoms during optimization are very large (>200 pm). Even though we are not able to locate a clear "transition state", we nevertheless think the results are illustrative.

The energy profile of the forward transition starting with α-cristobalite SiO$_2$ displays a maximum barrier of 1.17 eV/f.u. This is only slightly lower than $\Delta H_{a,fwd} = 1.28$ eV/f.u. computed for the (regular) cation method. Interestingly, the forward transformation did not yield the stishovite SiO$_2$ structure. Instead, it left the $C222_1$ path early on, coinciding with a non-orthogonal cell at the maximum energy. Each Si atom still gained two additional bonds, but those were provided from different O in comparison to the cation method. The final structure adopts monoclinic symmetry (SpGr. $P2_1$ (4)) [53] with yet another ordered arrangement of SiO$_6$ octahedra. It bears resemblance to sei-fertite-SiO$_2$ [44], although the agreement is not perfect. Its energy comes out as 0.1 eV/SiO$_2$ higher than that of seifertite-SiO$_2$.

The other profile in Fig. 7 corresponds to the reverse transition, starting with stishovite SiO$_2$. The profile is noticeably different from the graph shown in Fig. 6, which was the result of a concerted movement of all cations. We find that the stishovite structure ruptures already at an "activation" of barely 0.22 eV/f.u., significantly lower than the activation barrier of 0.71 eV/f.u. computed for transformation from stishovite to cristobalite following the $C222_1$ path in the cation method. At the first cusps (from step 16 to 15) cations lose one bond to O, becoming 5-coordinated. At the second cusp (from step 11 to 10), they lose yet another bond to O and major displacements up to 200 pm occur in the structure. The outcome is not cristobalite, but an arrangement of four- and eight membered rings of corner-sharing SiO$_4$ tetrahedra in a non-

rectangular cell. Its relation to the cristobalite structure is unclear to us. However, it may only take a relatively small amount of bond re-arrangements to relate both structures. Such mechanisms are known among polymorphs of SiO$_2$, for example, for the tridymite to keatite transition [54].

The results above show, although the idealized structures were not reached, that cristobalite naturally transforms into a structure with SiO$_6$ octahedra upon compression. Indeed, ab-initio molecular dynamics simulation show that α-cristobalite-SiO$_2$ transforms into stishovite-SiO$_2$ at high pressure, with intermediates described within $C222_1$ symmetry [19]. We reproduced the results using the same small simulation cell as in the original study. However, extending the simulation cell to twice its size produced disordered models comprising SiO$_6$ octahedra rather than stishovite. Conversely, the transition paths show that upon expansion stishovite transforms into a structure with SiO$_4$ tetrahedra. Adding more degrees of freedom produced slightly lower activation barriers, indicating that our values we present in Tables 4, 5, and 6 can be considered as upper boundaries. Even though the idealized structures were not reached, it is conceivable that in an experiment further annealing of a disordered compound under compressive or tensile stress yields crystalline samples.

4. Conclusions

Increasing pressure increases the relative stability of the rutile-type over the cristobalite-type for SiO$_2$, GeO$_2$, and TiO$_2$. While for SiO$_2$ the rutile-type succeeds the cristobalite-type at high pressures, we show that for GeO$_2$ and TiO$_2$, where the rutile-type is an ambient pressure modification, the cristobalite-type is attainable at small negative pressures. Our investigation of transition paths show that increasing pressure yields lower activation barriers for a transformation from cristobalite-type to rutile-type. The activation barrier of the reverse transformation, from rutile-type into cristobalite-type, decreases with decreasing pressure. Following concerted movements of atoms, we show that the cation method of Salvadó et al. [21] yields lower activation barriers than a concerted movement of anions. Even smaller barriers are encountered if only a subset of cations is moved. The resulting structures in these "half cation methods" for both forward and reverse paths still display octahedral or tetrahedral coordination of all cations but may not match rutile or cristobalite structures.

Given that the magnitude of negative pressure at which cristobalite-GeO$_2$ and cristobalite-TiO$_2$ become thermodynamically stable is only 1 to 3 GPa, we propose to prepare experiments that utilize tensile stresses of this magnitude. For example, rutile-type GeO$_2$ or TiO$_2$ may be deposited as thin film on a curved substrate, which is then relaxed. Subsequent annealing at moderate temperatures may yield a crystalline tetrahedrally coordinated structure. Two new compounds with potentially interesting properties are in reach through relatively simple synthetic pathways.

CRediT authorship contribution statement

Shariq Haseen: Conceptualization, Data curation, Formal analysis, Investigation, Methodology, Resources, Software, Validation, Visualization, Writing - original draft. **Peter Kroll:** Conceptualization, Data curation, Formal analysis, Investigation, Methodology, Resources, Software, Validation, Visualization, Funding acquisition, Project administration, Supervision, Writing - original draft.

Acknowledgements

Declaration of Competing Interest

There are no conflicts to declare.

Data availability

The raw/processed data required to reproduce these findings cannot be shared at this time due to technical or time limitations.

References

[1] A.F. Wells, Structural Inorganic Chemistry, Clarendon Press, Oxford, 1975.
[2] A.J. Leadbetter, A.F. Wright, Philos. Mag. 33 (1976) 105–112.
[3] S.M. Stishov, S.V. Popova, Geokhimiya 10 (1961) 837–839.
[4] E.C.T. Chao, J.J. Fahey, J. Littler, D.J. Milton, J. Geophys. Res. 67 (1962) 419–421.
[5] H. Böhm, Naturwissenschaften 55 (1968) 648–649.
[6] E. Hauser, H. Nowotny, K.J. Seifert, Monatsh. Chem. 101 (1970) 715–720.
[7] O. Yamaguchi, K. Kotera, M. Asano, K. Shimizu, J. Chem. Soc. Dalton Trans. (1982) 1907–1910.
[8] P. Degryse, J. Elsen, in: Leuven University Press, Leuven, Belgium, 2003, pp. 120.
[9] J.M. Léger, J. Haines, M. Schmidt, J.P. Petitet, A.S. Pereira, J.A.H. da Jornada, Nature 383 (1996) 401.
[10] M. Micoulaut, L. Cormier, G.S. Henderson, J. Phys.: Condens. Matter 18 (2006) R753–R784.
[11] M. Sahnoun, C. Daul, R. Khenata, H. Baltache, Eur. Phys. J. B Conden. Matter Complex Syst. 45 (2005) 455–458.
[12] L. Vegard, London Edinburgh Dublin Philos. Mag. J. Sci. 32 (1916) 505–518.
[13] R.E. Day, Prog. Org. Coat. 2 (1973) 269.
[14] D.H. Solomon, D.G. Hawthorne, Chemistry of Pigments and Fillers, John Wiley, New York, 1983.
[15] Y. Cao, T. He, Y. Chen, Y. Cao, J. Phys. Chem. C 114 (2010) 3627–3633.
[16] D. Deng, M.G. Kim, J.Y. Lee, J. Cho, Energy Environ. Sci. 2 (2009) 818–837.
[17] M. O'Keefe, B.G. Hyde, Acta Crystallogr. Sect. B 32 (1976) 2923–2936.
[18] B. Silvi, L.H. Jolly, P. D'Arco, J. Mol. Struct. (Thoechem) 260 (1992) 1–9.
[19] D.D. Klug, R. Rousseau, K. Uehara, M. Bernasconi, Y. Le Page, J.S. Tse, Phys. Rev. B 63 (2001) 104106.
[20] L. Huang, M. Durandurdu, J. Kieffer, Nat. Mater. 5 (2006) 977.
[21] M.A. Salvadó, P. Pertierra, A. Morales-García, J.M. Menéndez, J.M. Recio, J. Phys. Chem. C 117 (2013) 8950–8958.
[22] T. Moon, P. Kroll, J. High School Res. 1 (2010) 20–25.
[23] G. Kresse, J. Hafner, Phys. Rev. B 47 (1993) 558–561.
[24] G. Kresse, J. Hafner, Phys. Rev. B 49 (1994) 14251–14269.
[25] G. Kresse, J. Furthmüller, Comput. Mater. Sci. 6 (1996) 15–50.
[26] G. Kresse, J. Furthmüller, Phys. Rev. B 54 (1996) 11169–11186.
[27] J.P. Perdew, K. Burke, M. Ernzerhof, Phys. Rev. Lett. 77 (1996) 3865–3868.
[28] J.P. Perdew, K. Burke, M. Ernzerhof, Phys. Rev. Lett. 78 (1997) 1396.
[29] J. Sun, A. Ruzsinszky, J.P. Perdew, Phys. Rev. Lett. 115 (2015) 036402.
[30] P.E. Blöchl, Phys. Rev. B 50 (1994) 17953–17979.
[31] G. Kresse, D. Joubert, Phys. Rev. B 59 (1999) 1758–1775.
[32] H.J. Monkhorst, J.D. Pack, Phys. Rev. B 13 (1976) 5188–5192.
[33] R.W.G. Wyckoff, Am. J. Sci. 9 (1925) 448–459.
[34] D.C. Palmer, in, CrystalMaker Software Ltd, Begbroke, Oxfordshire, England, 2014.
[35] J.B. Parise, A. Yeganeh-Haeri, D.J. Weidner, J.D. Jorgensen, M.A. Saltzberg, J. Appl. Phys. 75 (1994) 1361–1367.
[36] K.J. Seifert, H. Nowotny, E. Hauser, J. Monatshefte für Chemie/Chem. Month. 102 (1971) 1006–1009.
[37] M. Sugiyama, S. Endo, K. Koto, Mineral. J. 13 (1987) 455–466.
[38] J. Haines, J.M. Léger, C. Chateau, A.S. Pereira, Phys. Chem. Miner. 27 (2000) 575–582.
[39] S.C. Abrahams, J.L. Bernstein, J. Chem. Phys. 55 (1971) 3206–3211.
[40] H. Peng, Z. Yang, J. Sun, J.P. Perdew, ArXiv e-prints, 2016. arXiv:1510.05712.
[41] H. Kim, J.-M. Choi, W.A. Goddard, J. Phys. Chem. Lett. 3 (2012) 360–363.
[42] N. Khosrovani, A.W. Sleight, J. Solid State Chem. 121 (1996) 2–11.
[43] Y. Tsuchida, T. Yagi, Nature 347 (1990) 267–269.
[44] T. Kubo, T. Kato, Y. Higo, K.-I. Funakoshi, Sci. Adv. 1 (2015) e1500075.
[45] A. Černok, K. Marquardt, R. Caracas, E. Bykova, G. Habler, H.-P. Liermann, M. Hanfland, M. Mezouar, E. Bobocioiu, L. Dubrovinsky, Nat. Commun. 8 (2017) 15647.
[46] S. Saito, T. Ono, Japan. J. Appl. Phys. 50 (2011) 02153-02151 - 021503-021505.
[47] J. Haines, O. Cambon, E. Philippot, L. Chapon, S. Hull, J. Solid State Chem. 166 (2002) 434–441.
[48] A.W. Laubengayer, D.S. Morton, J. Am. Chem. Soc. 54 (1932) 2303–2320.
[49] S. Siol, A. Holder, J. Steffes, L.T. Schelhas, K.H. Stone, L. Garten, J.D. Perkins, P.A. Parilla, M.F. Toney, B.D. Huey, W. Tumas, S. Lany, A. Zakutayev, Sci. Adv. 4 (2018) eaaq1442.
[50] D.R. McKenzie, D. Muller, B.A. Pailthorpe, Phys. Rev. Lett. 67 (1991) 773–776.
[51] J.W. Ager, S. Anders, A. Anders, I.G. Brown, Appl. Phys. Lett. 66 (1995) 3444–3446.
[52] A.J. Gratz, L.D. DeLoach, T.M. Clough, W.J. Nellis, Science 259 (1993) 663–666.
[53] H.T. Stokes, D.M. Hatch, J. Appl. Crystallogr. 38 (2005) 237–238.
[54] C.-T. Li, Acta Crystallogr. Sect. B 27 (1971) 1132–1140.